

NUCLEOSYNTHESIS IN ELECTRON CAPTURE SUPERNOVAE OF AGB STARS

S. WANAJO^{1, 2}, K. NOMOTO^{1, 2}, H. -T. JANKA³, F. S. KITAJURA³, AND B. MÜLLER³

Draft version November 3, 2018

ABSTRACT

We examine nucleosynthesis in the electron capture supernovae of progenitor AGB stars with an O-Ne-Mg core (with the initial stellar mass of $8.8 M_{\odot}$). Thermodynamic trajectories for the first 810 ms after core bounce are taken from a recent state-of-the-art hydrodynamic simulation. The presented nucleosynthesis results are characterized by a number of distinct features that are not shared with those of other supernovae from the collapse of stars with iron core (with initial stellar masses of more than $10 M_{\odot}$). First is the small amount of ^{56}Ni ($= 0.002 - 0.004 M_{\odot}$) in the ejecta, which can be an explanation for observed properties of faint supernovae such as SNe 2008S and 1997D. In addition, the large Ni/Fe ratio is in reasonable agreement with the spectroscopic result of the Crab nebula (the relic of SN 1054). Second is the large production of ^{64}Zn , ^{70}Ge , light *p*-nuclei (^{74}Se , ^{78}Kr , ^{84}Sr , and ^{92}Mo), and in particular, ^{90}Zr , which originates from the low Y_e ($= 0.46 - 0.49$, the number of electrons per nucleon) ejecta. We find, however, that only a 1 – 2% increase of the minimum Y_e moderates the overproduction of ^{90}Zr . In contrast, the production of ^{64}Zn is fairly robust against a small variation of Y_e . This provides the upper limit of the occurrence of this type of events to be about 30% of all core-collapse supernovae.

Subject headings: nuclear reactions, nucleosynthesis, abundances — stars: abundances — supernovae: general — supernovae: individual (SN 1054, SN 1997D, SN 2008S) — nebulae: Crab Nebula

1. INTRODUCTION

Massive stars end their lives with core-collapse supernovae (SNe II/Ibc), which are the predominant sources of having enriched galaxies with the elements heavier than helium. The other type, thermonuclear supernovae (SNe Ia), also contributes to the enrichment of iron-peak elements, which is, however, absent in the early universe. The metals produced by core-collapse supernovae serve as diagnostic tools to uncover the chemical-enrichment history of the Galaxy from its poorly understood early stage to the present day. A reliable prediction of supernova yields has been, however, hampered by the yet unknown mechanism that causes the explosion. Previous studies of supernova nucleosynthesis have relied upon a number of model parameters such as the explosion energy, the position that divides the ejecta and the remnant (mass cut), and the electron fraction (Y_e , the number of electrons per nucleon). The production of each element in a supernova, in particular of those synthesized in the innermost ejecta, is severely affected by the choice of these parameters (see, e.g., Tominaga et al. 2007; Heger & Woosley 2008). It is obvious that nucleosynthesis studies with self-consistently exploding models are eventually needed to obtain reliable supernova yields.

Recent one-dimensional simulations including accurate neutrino transport seem to exclude the pos-

sibility of neutrino-driven explosions without the help of multi-dimensional effects (Rampp & Janka 2000; Mezzacappa et al. 2001; Liebendörfer et al. 2001; Thompson et al. 2003; Sumiyoshi et al. 2005; Buras et al. 2006), at least for standard nuclear and neutrino physics input. An exception are the explosions of $8 - 10 M_{\odot}$ stars. A star in this mass range forms an electron-degenerate core consisting of oxygen, neon, and magnesium (O-Ne-Mg) during the final stage of its evolution (instead of an iron core in the case of more massive stars), and becomes a super asymptotic giant branch (AGB) star. Such a star ends its life either as an O-Ne-Mg white dwarf or a core-collapse supernova leaving behind a neutron star. For the latter, the collapse is induced by electron capture (what is called an “electron capture supernova”) when the core mass grows to $1.38 M_{\odot}$ and the central density reaches $4 \times 10^9 \text{ g cm}^{-3}$. However, the uncertainties in mixing and mass loss during the evolution make it difficult to draw a clear line between these two channels (Nomoto 1984, 1987). Recent studies report that only the range close to the upper end (a mass range of $\lesssim 1 M_{\odot}$ or $\sim 4\%$ of all supernovae, Siess 2007; Poelarends et al. 2008) leads to the explosion channel, although the range could be wider for lower metallicity stars.

The structure of the O-Ne-Mg core is distinctively different from the iron cores of more massive stars by the fact that it has a steep density gradient in the outermost layers, surrounded by an extremely extended, loosely bound H/He envelope. Recently, Kitaura et al. (2006) have obtained self-consistent explosions from the collapse of the O-Ne-Mg core in a stellar progenitor with an initial mass of $8.8 M_{\odot}$ developed by Nomoto (1984). Their one-dimensional simulations with a state-of-the-art, energy-dependent treatment of the neutrino transport are in

¹ Institute for the Physics and Mathematics of the Universe, University of Tokyo, Kashiwa, Chiba 277-8582, Japan

² Department of Astronomy, School of Science, University of Tokyo, Bunkyo-ku, Tokyo, 113-8654, Japan; wana.jo@astron.s.u-tokyo.ac.jp, nomoto@astron.s.u-tokyo.ac.jp

³ Max-Planck-Institut für Astrophysik, Karl-Schwarzschild-Str. 1, D-85748 Garching, Germany; thj@mpa-garching.mpg.de, kitaura@mpa-garching.mpg.de

fact the only recent models in the literature with successful supernova explosions in spherical symmetry for standard nuclear and weak interaction physics (see also Burrows et al. 2007, for a similar result). The explosions are initiated by the rapid outward acceleration of the supernova shock when it encounters the steep density gradient and fast decline of the mass accretion rate at the edge of the O-Ne-Mg core. They are powered by the neutrino-heating mechanism, which yields a low explosion energy of $\sim 1\text{--}2 \times 10^{50}$ erg (for a detailed discussion, see Janka et al. 2008a). The new calculations are a revision of previous hydrodynamic results for the same O-Ne-Mg core, namely, of prompt explosions (Hillebrandt et al. 1984; Wanajo et al. 2003), powerful neutrino-driven explosions ($0.6 - 1.2 \times 10^{51}$ erg, Mayle & Wilson 1988), and no explosions (Burrows & Lattimer 1985; Baron, Cooperstein, & Kahana 1987).

The purpose of this paper is to present nucleosynthesis results for the first 810 ms of the neutrino-driven explosion of a collapsing O-Ne-Mg core (electron capture supernova), using the thermodynamic trajectories obtained by Kitaura et al. (2006). Employing a self-consistently calculated explosion model with sophisticated neutrino transport is of particular importance not only for the nucleosynthesis study itself, but also for a couple of other aspects. On the one hand, the mass range of 8–10 M_{\odot} accounts for about 30% of all the core-collapse supernova events, if all the range leads to the explosion channel. The electron capture supernovae can thus be potentially significant contributors to the Galactic chemical evolution of some species. On the other hand, explosions from these progenitors have been proposed as a possible explanation for the inferred low explosion energy of SN 1054 (Crab supernova, Nomoto et al. 1982; Davidson et al. 1982) (see also Hillebrandt 1982, for the 10 M_{\odot} progenitor with an iron core) as well as for the small ^{56}Ni amount estimated for some low-luminosity supernovae (e.g., SN 1997D, Turatto et al. 1998; Chugai & Utrobin 2000; Benetti et al. 2001; Hendry et al. 2005). A newly identified class of luminous transients like SN 2008S, whose progenitors were deeply dust-enshrouded massive stars, is also suggested to be electron capture supernovae (Prieto et al. 2008; Thompson et al. 2008) (see also Pastorello et al. 2007).

Recently, Hoffman et al. (2008) have investigated the nucleosynthesis in electron capture supernovae, using an explosion calculation of Janka et al. (2008a) that is very similar to the explosion models of Kitaura et al. (2006) (but was computed with slightly different input physics, see Janka et al. 2008a). Their study was aimed at determining whether the conditions are suitable for an r -process. They found no r -process formation and a severe overproduction of ^{90}Zr , which is also seen in our results. In our work, however, we perform nucleosynthesis calculations in much more detail, taking into account a number of possible uncertainties. In the following section (§ 2) the explosion models of Kitaura et al. (2006) and the methods for the nucleosynthesis calculations will be described. The nucleosynthesis results for the original model and for various modifications of it will be presented in § 3. We will discuss the question whether electron capture supernovae can be significant contributors to Galactic chemical evolution in § 4 and will address the

possibility that they are the origin of some low-energy supernovae in § 5. Finally, our summary and conclusions will follow in § 6.

2. EXPLOSION MODEL AND REACTION NETWORK

Kitaura et al. (2006) have simulated the collapse of the O-Ne-Mg core (with the mass of $1.38 M_{\odot}$, Nomoto 1984) (see also Miyaji et al. 1980), employing two different (“soft” and “stiff”) nuclear equations of state (EoSs). In this study, we adopt the result with the softer EoS (Lattimer & Swesty 1991, LS) as the “standard” model (labelled ST), which is qualitatively similar to that with the stiffer one (WH; Wolff & Hillebrandt EoS in Hillebrandt et al. 1984). The model with the WH EoS is used later for the purpose of comparison (§ 3.2). Figure 1 shows the evolution of the radius, density, temperature, and Y_e for selected mass elements in model ST as a function of post-bounce time t_{pb} . The ejecta in model ST are split into 29 mass shells with the first ejected zone having a mass of about $4 \times 10^{-4} M_{\odot}$ and each of the other ones of about $5 \times 10^{-4} M_{\odot}$ ($1.39 \times 10^{-2} M_{\odot}$ in total).

The nucleosynthesis yields in each mass shell are obtained in a post-processing step by solving an extensive nuclear reaction network code. The network consists of 6300 species between the proton- and neutron-drip lines predicted by the recent fully microscopic mass formula (HFB-9, Goriely et al. 2005), all the way from single neutrons and protons up to the $Z = 110$ isotopes. All relevant reactions, i.e. (n, γ) , (p, γ) , (α, γ) , (p, n) , (α, n) , (α, p) , and their inverses are included. The experimental data, whenever available, and the theoretical predictions for light nuclei ($Z < 10$) are taken from the REACLIB⁴ compilation. All the other reaction rates are taken from the Hauser-Feshbach rates of BRUSLIB⁵ (Aikawa et al. 2005) making use of experimental masses (Audi, Wapstra, & Thibault 2003) whenever available or the HFB-9 mass predictions (Goriely et al. 2005) otherwise. The photodisintegration rates are deduced from the reverse rates applying the reciprocity theorem with the nuclear masses considered. The weak and intermediate screening corrections to charged particle reactions are adopted from Graboske et al. (1973).

The β -decay rates are taken from the gross theory predictions (GT2, Tachibana, Yamada, & Yoshida 1990) obtained with the HFB-9 predictions (T. Tachibana 2005, private communication). Electron capture reactions on free nucleons and on heavy nuclei (Fuller, Fowler, & Newman 1982; Langanke & Martinez-Pinedo 2001) as well as rates for neutrino capture on free nucleons and ^4He and for neutrino spallation of free nucleons from ^4He (Woosley et al. 1990; McLaughlin, Fuller, & Wilson 1996) are also included. In contrast, neutrino-induced reactions of heavy nuclei are not taken into account in this study, but they are expected to make only minor effects (Meyer, McLaughlin, & Fuller 1998). Figure 2 shows the luminosities and mean energies for neutrinos of all types as functions of the post-bounce time t_{pb} in model ST; these results are taken from Kitaura et al. (2006) and used for calculating the rates of neutrino-induced reactions. More precisely, we should apply

⁴ <http://nucastro.org/reactlib.html>.

⁵ <http://www.astro.ulb.ac.be/Html/bruslib.html>.

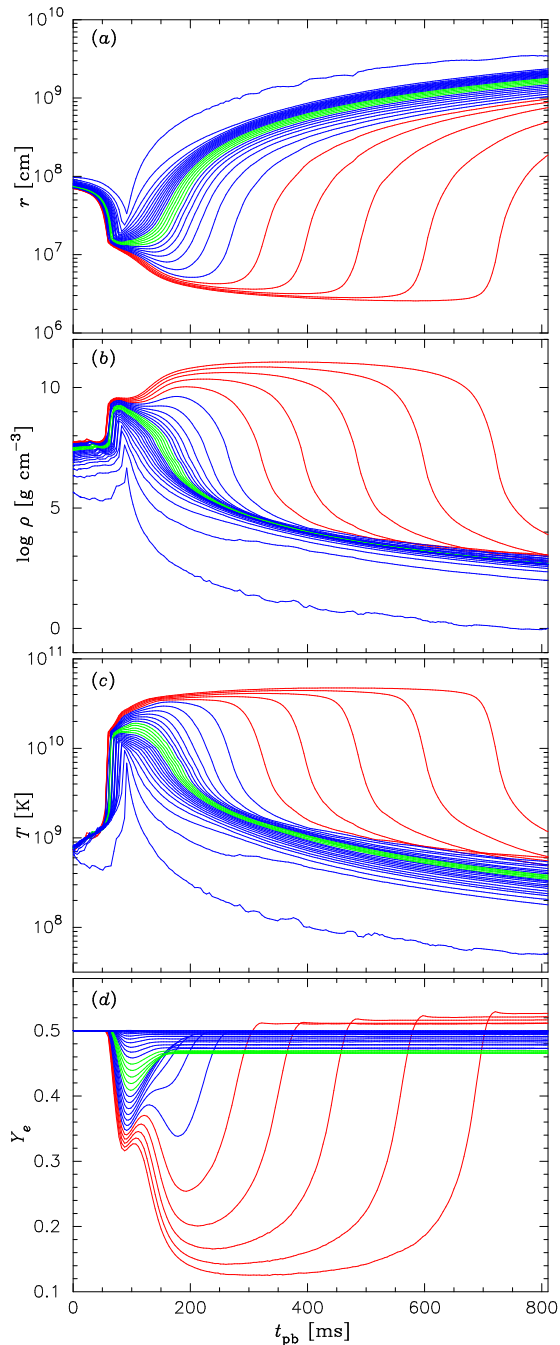


FIG. 1.— Radius (a), density (b), temperature (c), and Y_e (d) as a function of post-bounce time for material ejected from the collapsing O-Ne-Mg core in model ST. The trajectories are colored in green, blue, and red for $Y_e < 0.470$, $0.470 < Y_e < 0.500$, and $Y_e > 0.500$ (values at the end of simulation), respectively.

those quantities in the co-moving frame of the fluid with corrections for the gravitational redshift and for Doppler shifting due to fluid motion. We neglect such effects, which are important on the one hand only when the fluid is relatively close to the neutrino sphere ($< \text{several } 10 \text{ km}$), where the temperature is still higher than $T_9 = 9$ (see below). On the other hand, at large distances, where the expansion velocities of the gas are larger, neutrino interactions become essentially irrelevant.

Each nucleosynthesis calculation is initiated when the

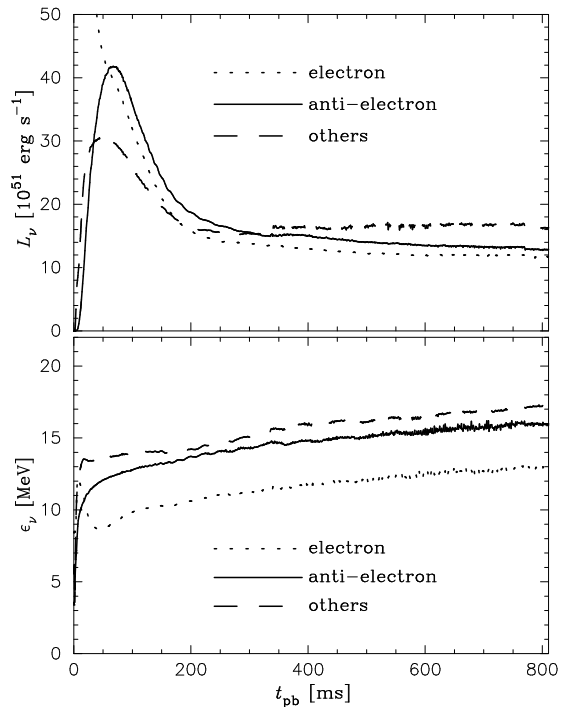


FIG. 2.— Neutrino luminosities (top) and mean neutrino energies (bottom) as functions of post-bounce time for electron (dotted line), anti-electron (solid line), and heavy-lepton (dashed line) neutrinos. The data are given for an observer at rest at 400 km from the center.

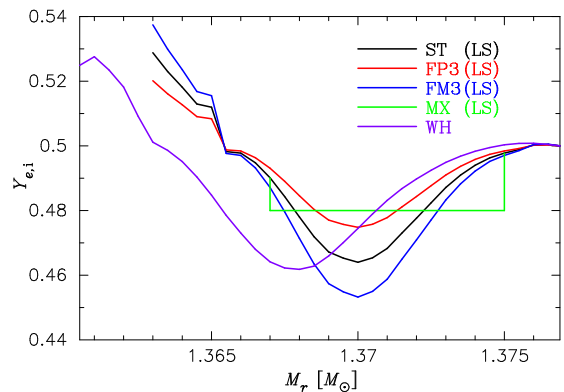


FIG. 3.— Initial electron fraction $Y_{e,i}$ for material ejected from the core as a function of the enclosed mass, M_r . Different colors correspond to models ST, FP3, FM3, MX, and WH as denoted in the panel (see text).

temperature decreases to $T_9 = 9$ (where $T_9 \equiv T/10^9 \text{ K}$). In the first ejected trajectory, the highest temperature is $T_9 \approx 7$ (Fig. 1), which is taken to be the initial condition for this case only. At such high temperatures, the composition is in the nuclear statistical equilibrium (mostly free nucleons and few α particles), which is realized immediately after the calculation starts. The initial compositions is then given by $X_n = 1 - Y_{e,i}$ and $X_p = Y_{e,i}$, respectively, where X_n and X_p are the mass fractions of free neutrons and protons, and $Y_{e,i}$ is the initial electron fraction at $T_9 = 9$ (Fig. 3, black line for model ST).

3. NUCLEOSYNTHESIS RESULTS

In subsection 3.1, we will present the nucleosynthesis results for the unmodified model (ST) of Kitaura et al. (2006), and the corresponding information for variations

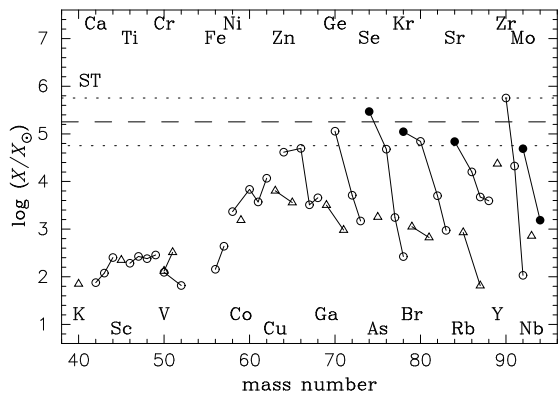


FIG. 4.— Mass fractions of isotopes (after decay) in the ejecta of model ST relative to their solar values (Lodders 2003) as functions of mass number. The abundances smaller than $X/X_{\odot} < 40$ are omitted. The even- Z and odd- Z isotopes are denoted by open circles and triangles, respectively. The p -nuclei are represented with filled symbols. The solid lines connect isotopes of a given element. The dotted horizontal lines indicate a “normalization band” between the largest production factor and a factor of ten smaller than that, along with the median value (*dashed line*).

of model ST will then be discussed in the following subsections. In each model, the nucleosynthetic yields for all the trajectories are mass-integrated over the ejecta-mass range.

3.1. Unmodified Model

The nucleosynthesis results of the unmodified model (ST) are shown in Figures 4 (isotopes) and 5 (elements). Both plots present the overproduction factors defined by the mass fractions in the ejecta with respect to their solar values (Lodders 2003). The even- Z and odd- Z species are denoted by circles and triangles, respectively. In Figure 4, the isotopes for a given element are connected by lines, and the abundances smaller than $X/X_{\odot} < 40$ are omitted. The dotted horizontal lines indicate a “normalization band” between the largest production factor (^{90}Zr and Zr in Figs. 4 and 5, respectively) and a factor of ten smaller than that, along with the median value (*dashed line*). This band is taken to be representative of the uncertainty in the nuclear data involved. In the following, we consider that electron capture supernovae can be contributors to the solar (or Galactic) inventories of the species located within the normalization band.

Figure 4 indicates that, along with the marginal ones, model ST can account for the production of $^{64,66}\text{Zn}$, ^{70}Ge , $^{74,76}\text{Se}$, $^{78,80}\text{Kr}$, ^{84}Sr , ^{90}Zr , and ^{92}Mo , where all the light p -nuclei (*filled circles*) up to $A = 92$ are included. However, only a few elements (Zn, Ge, Y, and Zr) fall into the normalization band (Fig. 5), since the p -nuclei comprise only small fractions of a given element (0.89%, 0.35%, 0.56%, and 14.8% for ^{74}Se , ^{78}Kr , ^{84}Sr , and ^{92}Mo , respectively). Our result for model ST is in reasonable agreement with that in Hoffman et al. (2008, Fig. 1)⁶, and some differences are due to the slightly higher minimum Y_e in our model (§ 3.5).

Figure 6 shows the mass fractions of some important isotopes (after decay) for model ST (*top*) and these mass

⁶ The total ejecta mass including the outer H/He envelope is taken to be $1.263 M_{\odot}$ in Hoffman et al. (2008), while we consider only the calculated zones with $1.39 \times 10^{-2} M_{\odot}$. This leads to the hundred times larger values of X/X_{\odot} in this paper.

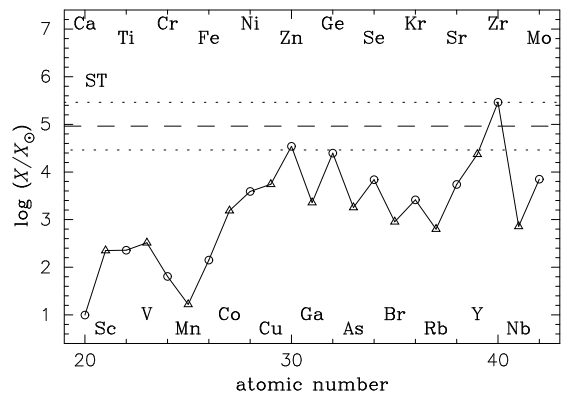


FIG. 5.— Mass fractions of elements (after decay) in the ejecta of model ST relative to their solar values (Lodders 2003) as a function of atomic number. The even- Z and odd- Z elements are denoted by open circles and triangles, respectively.

fractions relative to their solar values (*bottom*) as functions of the enclosed mass M_r . In each mass shell, the dominant heavy isotope is either ^{56}Fe (produced in the form of ^{56}Ni) or $^{58,60}\text{Ni}$, depending on $Y_{e,i}$. In the neutron-rich ejecta, the nuclear products in the single quasi-statistical-equilibrium (QSE) cluster have peaks at $A \sim 60$ and $A \sim 90$ because of the strong binding at $N = 28$ and 50 (Meyer, Krishnan, & Clayton 1998). The abundance of ^{90}Zr is maximal in the mass shell with the lowest $Y_{e,i} = 0.464$. In addition, the matter with $Y_{e,i} = 0.46 - 0.49$ is so *proton-rich* (compared to the average of the stable isotopes in the vicinity, e.g., the proton fraction of ^{90}Zr is 0.44) that the successive proton captures lead to the production of light p -nuclei up to $A = 92$. This can also be seen in the early neutrino-driven winds (Hoffman et al. 1996; Wanajo 2006).

It should be noted that such a nucleosynthesis result that stems from the low- Y_e ($\sim 0.47 - 0.49$) matter in the early ejecta may be a unique characteristics of collapsing O-Ne-Mg cores. In the present model, the explosion sets in immediately after core bounce and the ejecta rapidly expand, where the ejection of low Y_e matter seems unavoidable (see Fig. 1). For more massive progenitors ($> 10 M_{\odot}$), the explosion is expected to be more delayed and to eject neutrino-processed matter, where the bulk of the ejecta may have $Y_e \gtrsim 0.5$ (Fröhlich et al. 2006; Buras et al. 2006).

As will be discussed in § 4, the maximum overproduction factor of $X/X_{\odot} = 5.7 \times 10^5$ for model ST (Fig. 4) poses a severe constraint on the occurrence of this type of events to be no more than 1% of all core-collapse supernovae. This is in agreement with the conclusions by Hoffman et al. (2008). In the simulation of Kitaura et al. (2006) (also Janka et al. 2008a), the deceleration of the shock in the outer envelope slows the expansion of the ejecta only slightly. Therefore we do not expect any substantial fallback of the once ejected matter onto the remnant, as it is presumed to take place in the case of more massive progenitors (e.g., Umeda & Nomoto 2002). In the following subsections we thus explore possible modifications to model ST, which instead of fallback might provide a solution for moderating the extremely large overproduction of, in particular, ^{90}Zr .

3.2. Uncertainty in the Equation of States

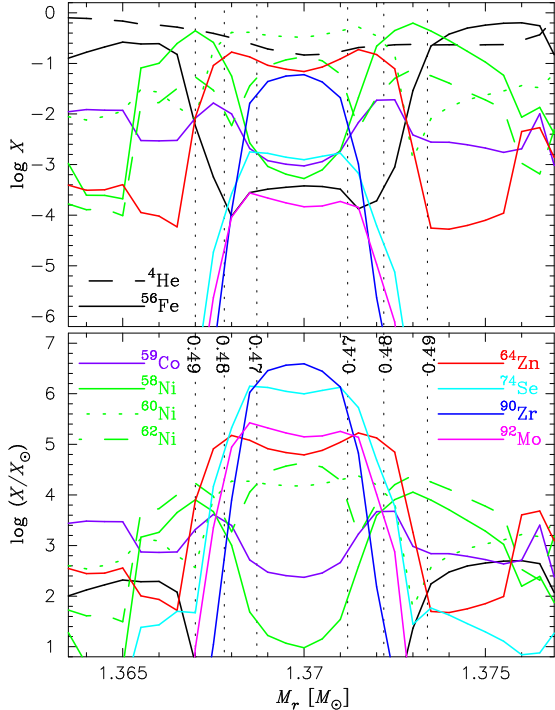


FIG. 6.— Mass fractions of several important isotopes (after decay) in the ejecta of model ST (*top*), and these mass fractions relative to their solar values (*bottom*) as functions of the enclosed mass M_r . The vertical dotted lines indicate the mass coordinates where the initial $Y_{e,i}$ is 0.470, 0.480, and 0.490 (see Fig. 3).

First, we examine nucleosynthesis in the explosion model calculated with the WH EoS in Kitaura et al. (2006). This model (hereafter WH) has thermodynamic trajectories very similar to those of model ST, but a slightly larger ejecta mass ($1.64 \times 10^{-2} M_\odot$) and a slightly lower minimal $Y_{e,i}$ ($= 0.462$). Another EoS by Shen et al. (1998), which is also currently available for core-collapse simulations, falls between the ST and WH EoSs in terms of its *stiffness* and a variety of results of core-collapse simulations, e.g. the radii of shock formation and stagnation or the size of the neutrino luminosities (see Janka et al. 2008b). Therefore, we suspect that a comparison of the nucleosynthesis results between models ST and WH well brackets the uncertainties arising from different EoSs.

All nucleosynthesis calculations are repeated with the thermodynamic trajectories and the initial compositions deduced from the $Y_{e,i}$ -mass profile (Fig. 3) of model WH. Figure 7a shows the mass fractions (*bottom*) in the ejecta for models ST and WH, along with their ratios X_{WH}/X_{ST} (*top*), as functions of the mass number A . Differences exceeding a factor of 2 (indicated by *dotted lines*) can be seen for the light species with $A < 20$. However, the differences are well below a factor of 2 for the dominant species in the vicinity of the QSE peaks at $A \approx 4, 60$, and 90. We therefore conclude that the uncertainties arising from different nuclear EoSs are not of great importance, at least for the currently available versions of EoSs. We note, however, that the WH EoS leads to a 60% larger ^{56}Ni mass than that for the LS EoS (Table 1). This suggests that EoSs play a crucial role to precisely determine the ^{56}Ni ejecta mass from an electron capture supernova.

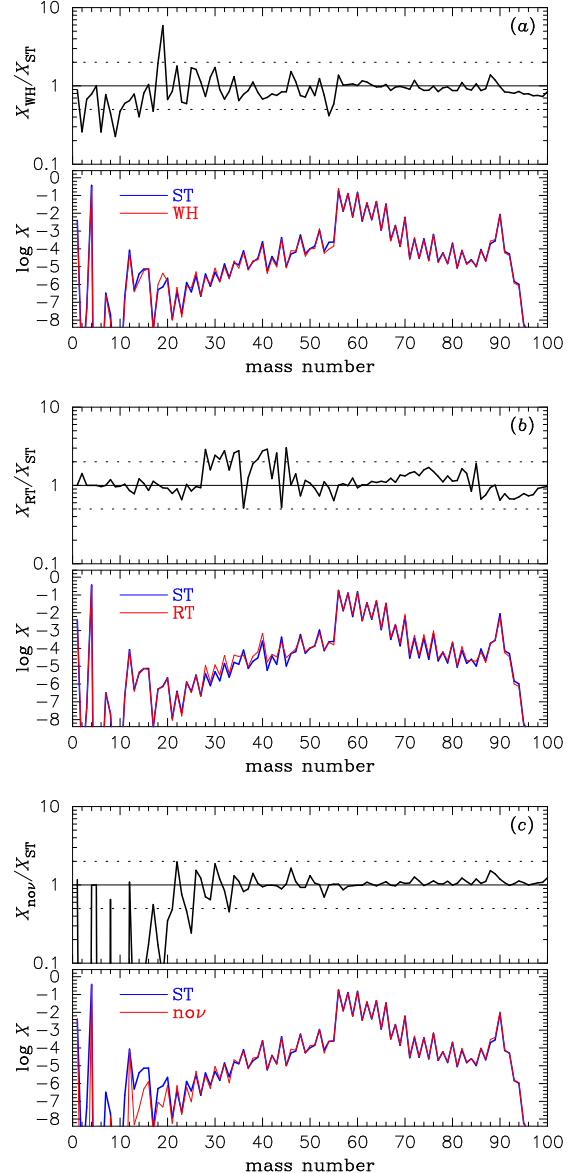


FIG. 7.— Mass fractions (*bottom* of each panel) in the ejecta for models ST (*blue*) and (a) WH, (b) RT, (c) *nov* (*red*; see the text), and their ratios (*top* of each panel), as functions of the mass number. In the top panels, a factor of 2 difference is indicated by dotted lines.

3.3. Uncertainty in the Nuclear Reaction Rates

In all the present calculations, the nucleosynthetic flows proceed along or in the vicinity of the β -stability line, forming the QSE peaks at $A \approx 4, 60$, and 90. The nuclear masses of relevance, which are the most important factors in this case, are measured with high enough accuracy (Audi, Wapstra, & Thibault 2003). Therefore, we do not expect a sizable change of the nucleosynthesis result arising from the uncertainties in nuclear reaction rates.

As a test, we repeat all the nucleosynthesis calculations of model ST with the theoretical rates (Aikawa et al. 2005) replaced by those of Rauscher & Thielemann (2000). Both data sets are based on the statistical (Hauser-Feshbach) approach with the experimental masses whenever available, but with different theoretical

masses and different nuclear level densities. The results (labelled by RT) are compared to those of model ST in Figure 7b. Factors of 2 – 3 difference can be seen for the nuclei between $A = 27$ and 45 (Fig. 8, *top*), which have, however, very small mass fractions (*bottom*). The differences for dominant species around $A \approx 4, 60,$ and 90 are well below a factor of 2.

3.4. Effects of Convection

A potentially important effect that is lacking in the one-dimensional simulations of Kitaura et al. (2006) is convective mixing of the ejecta (see the results of a two-dimensional simulation of a collapsing O-Ne-Mg core in Janka et al. 2008b). Figure 8 shows the profiles of temperature (*top*), entropy (*middle*), and Y_e (*bottom*) versus mass at early times ($t_{\text{pb}} = 126, 150, 176, 200,$ and 228 ms) and at the end of the simulation ($t_{\text{pb}} = 810$ ms). We find a negative entropy gradient forming at a temperature high enough for α -processing ($T_9 > 3$, which is indicated by the dashed line in the top panel of Fig. 9). This can cause convective overturn and one might speculate that this could moderate the neutron-richness to some extent *before* the freezeout.

As a limiting case, we present the result with the initial composition being determined by the $Y_{e,i}$ -mass profile shown by the green line in Figure 3 (hereafter, model MX). We assume here that the ejecta between 1.367 and 1.375 M_\odot (indicated by vertical dotted lines in Fig. 9) get completely mixed on microscopic scales to have a mass-averaged constant $Y_{e,i}$ ($= 0.480$). We find that the species having the largest overproduction, i.e., ^{90}Zr in model ST, is replaced by ^{64}Zn with ten times smaller value in model MX (Fig. 9). The largest overproduction of Zr (as element) is replaced by that of Zn (Fig. 10). Because of the increased minimum value of $Y_{e,i}$ ($Y_{e,\text{min}} = 0.480$) the overproduction of ^{90}Zr becomes unimportant.

It should be noted, however, that a corresponding two-dimensional simulation (carried out until 262 ms after core bounce; see Janka et al. (2008b) and Müller and Janka 2008, in preparation) with the same initial O-Ne-Mg core does not show any such small-scale mixing. Instead, the accreted post-shock gas makes one quick overturn (fully developed convection with many overturns does not occur), after which the rising material in Rayleigh-Taylor mushrooms is directly ejected and self-similar expansion is quickly established. Hence, there may not be sufficient time for mixing and homogenization on small scales. As will be discussed in § 3.5, however, a slight increase of $Y_{e,\text{min}}$ (e.g., $\Delta Y_{e,i} = 0.004$; from 0.464 to 0.468) is already enough to significantly moderate the overproduction of ^{90}Zr . Therefore, partial mixing of the ejecta induced by convection might be sufficient to cure this overproduction problem.

The negative entropy gradient may have a variety of other effects. One is that the convective overturn could stretch the mean duration of the neutrino irradiation of ejected matter and could also lead to regions of ejecta with higher $Y_{e,i}$. In fact, a recent two-dimensional simulation with a more massive progenitor (15 M_\odot , Buras et al. 2006) shows that the bulk of the ejecta turns out to be proton-rich ($Y_e > 0.5$). In the present case, however, the convective overturn may not have exactly the same effects as in more massive pro-

genitors, because the steep density gradient of the O-Ne-Mg core with its transition to an extremely dilute H-rich envelope makes the core structure distinctively different from that of more massive stars. As a consequence, the supernova ejecta accelerate much faster than in more massive stars, and the convective pattern in the overturn region freezes out in the self-similar expansion more quickly. Therefore convective mixing is rather inefficient and, moreover, it is possible that the neutrino-heated bubbles rise so rapidly away from the neutrino-sphere that clumps of low- Y_e material get ejected, a possibility that may be anticipated from the bottom panel of Figure 8 (e.g., the red and green lines there). This might increase the overproduction of other $N = 50$ species (^{86}Kr , ^{87}Rb , ^{88}Sr , ^{89}Y). In fact, some neutron-rich blobs (down to $Y_e \approx 0.41$, but with a tiny mass) are found in the preliminary results of the mentioned two-dimensional simulation (Müller and Janka 2008, in preparation, see also Janka et al. 2008b).

It should be noted that even two-dimensional models with their constraint of axisymmetry may not yield a sufficiently accurate mass distribution of the ejecta as a function of Y_e . Such a sensitive information might ultimately require three-dimensional simulations to allow for reliable conclusions concerning nucleosynthesis yields and production factors.

3.5. Small Y_e Variation

From Figure 6 we conclude that the large overproduction of ^{90}Zr in model ST is mainly due to the neutron-rich ejecta with $Y_{e,i}$ between $Y_{e,\text{min}} = 0.464$ and 0.470. The demonstration in § 3.4 (Fig. 9) shows that boosting $Y_{e,\text{min}}$ to 0.480 indeed removes the overproduction of ^{90}Zr . Motivated by this result, we explore in this subsection that how much increase of $Y_{e,\text{min}}$ could cure this extreme overproduction problem. We repeat that the $Y_{e,i}$ values are obtained from state-of-the-art simulations with sophisticated, energy-dependent neutrino transport in Kitaura et al. (2006). Nevertheless it is a great challenge to determine Y_e to an accuracy of a few percent, because the neutron-to-proton ratio in the ejecta is established by a delicate competition of electron neutrino and antineutrino captures and their inverse reactions, in particular around the radius where the kinetic equilibrium of these processes breaks down because the rates become slower than the expansion rate of the accelerating ejecta (for a detailed discussion, see Fröhlich et al. 2006). Besides the limited numerical resolution (in particular of the neutrino energy spectra) a variety of other effects can be imagined to imply uncertainties at the percent level, for example the potential effects of convective mixing on microscopic scales (§ 3.4), future refinements in the employed microphysics (e.g., EoSs, neutrino interaction rates, electron captures rates), possible effects due to nonstandard neutrino properties (e.g., flavor oscillations in the supernova core), and the uncertainties associated with the stellar evolution calculations of 8–10 M_\odot stars.

In order to test small variations of $Y_{e,\text{min}}$, we examine nucleosynthesis for the trajectories of model ST but with the original $Y_{e,i}$ profile replaced by $Y_{e,i} + (0.500 - Y_{e,i}) \times f$. The multiplicative factor f is taken to be 0.1, 0.2, and 0.3 (hereafter, models FP1, FP2, and FP3). The $Y_{e,i}$ - M_r profiles of these models are similar, but each model

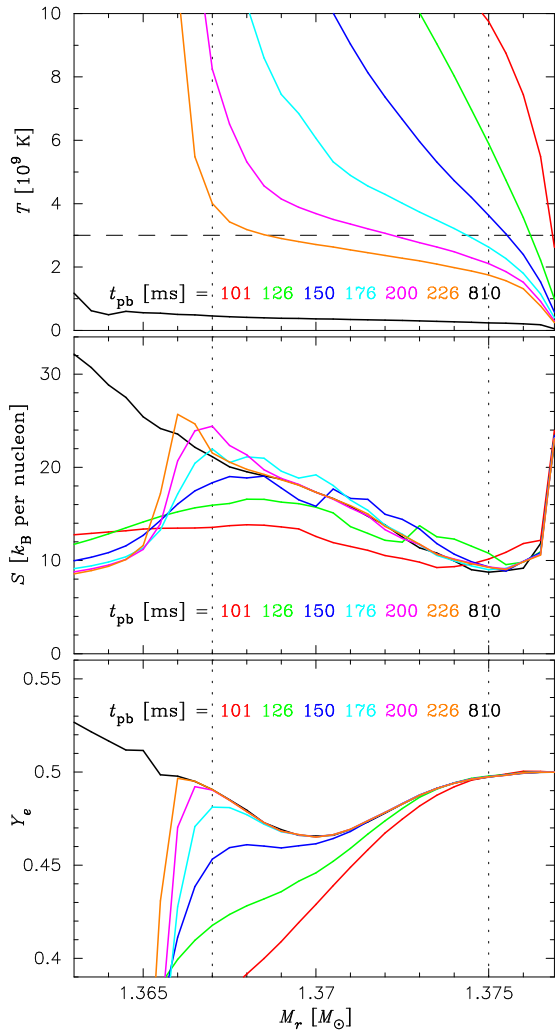


FIG. 8.— Profiles of temperature (*upper*), entropy (*middle*), and Y_e (*bottom*) versus enclosed mass M_r at early times ($t_{\text{pb}} = 100 - 230$ ms) and at the end of simulation ($t_{\text{pb}} = 810$ ms). See the text for the meaning of the vertical dotted lines and the horizontal dashed line.

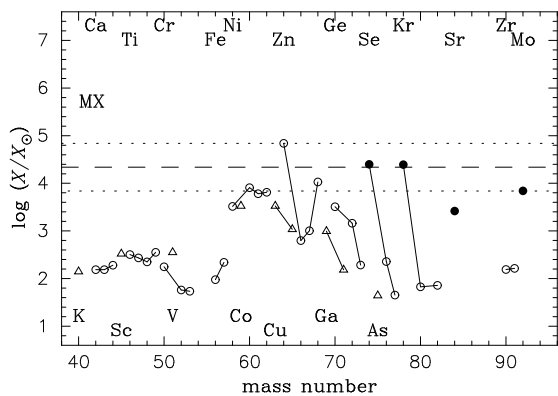


FIG. 9.— Same as Figure 4, but for model MX.

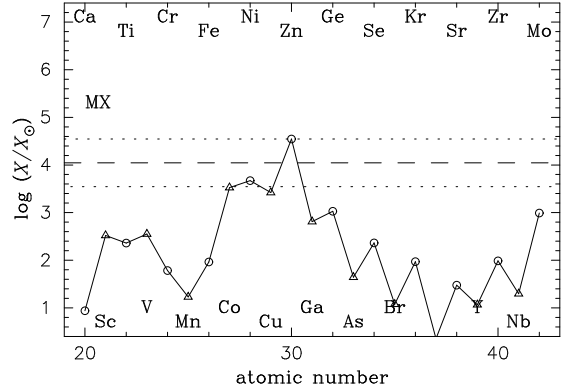


FIG. 10.— Same as Figure 5, but for model MX.

has a different $Y_{e,\text{min}}$ (see Fig. 3 for model FP3). The values of $Y_{e,\text{min}}$ for these models are slightly increased compared to that of model ST to be 0.468, 0.471, and 0.475, respectively (Table 1).

We find that the production of ^{90}Zr is extremely sensitive to $Y_{e,\text{min}}$ (Figure 11). The increase of $Y_{e,\text{min}}$ by only 1–2% ($\Delta Y_{e,i} = 0.004$ and 0.011 in models FP1 and FP3, respectively) reduces the production factor of ^{90}Zr by roughly two orders of magnitude. Other species like ^{64}Zn , ^{74}Se , and ^{78}Kr then possess the largest production factors. In the case of model FP3 these have one tenth of the values in model ST. Figure 12 indicates that electron capture supernovae could be the dominant sources of the elemental abundance of Zn, if such a slightly higher $Y_{e,i}$ was correct.

The results for $f = -0.1, -0.2,$ and -0.3 (hereafter, models FM1, FM2, and FM3) are shown in Figures 13 and 14. The values of $Y_{e,\text{min}}$ are then decreased to 0.460, 0.457, and 0.453, respectively (Table 1). The $Y_{e,i}-M_r$ profile for model FM3 is also displayed in Figure 3. The overproduction of ^{90}Zr becomes more serious in these models, and other $N = 50$ species (^{88}Sr and ^{89}Y) enter into the normalization band in the case of model FM3. The results of Hoffman et al. (2008, Fig. 1) resemble those for our model FM3 rather than those for model ST. This is probably explained by the fact that Hoffman et al. (2008) perform their evaluation for ejecta with a value of $Y_{e,\text{min}} = 0.454$, which is close to $Y_{e,\text{min}}$ in model FM3 ($= 0.453$), but slightly smaller than $Y_{e,\text{min}}$ in model ST. The small difference between the ejecta conditions in Hoffman et al. (2008) and those of model ST originates from a different density structure assumed for the dilute H/He envelope around the collapsing O-Ne-Mg core considered by Hoffman et al. (2008) (see Janka et al. 2008a, for more detail).

The results presented in this subsection imply that the overproduction of ^{90}Zr may not be as serious as reported by Hoffman et al. (2008), because an increase of $Y_{e,\text{min}}$ by only 2% cures this problem. This is a significant improvement compared to the situation in the older simulations by Mayle & Wilson (1988), where $Y_{e,\text{min}}$ was found to be around 0.4 and a substantial change ($\sim 20\%$) of $Y_{e,\text{min}}$ was necessary to avoid the overproduction of $N = 50$ nuclei.

3.6. νp -process

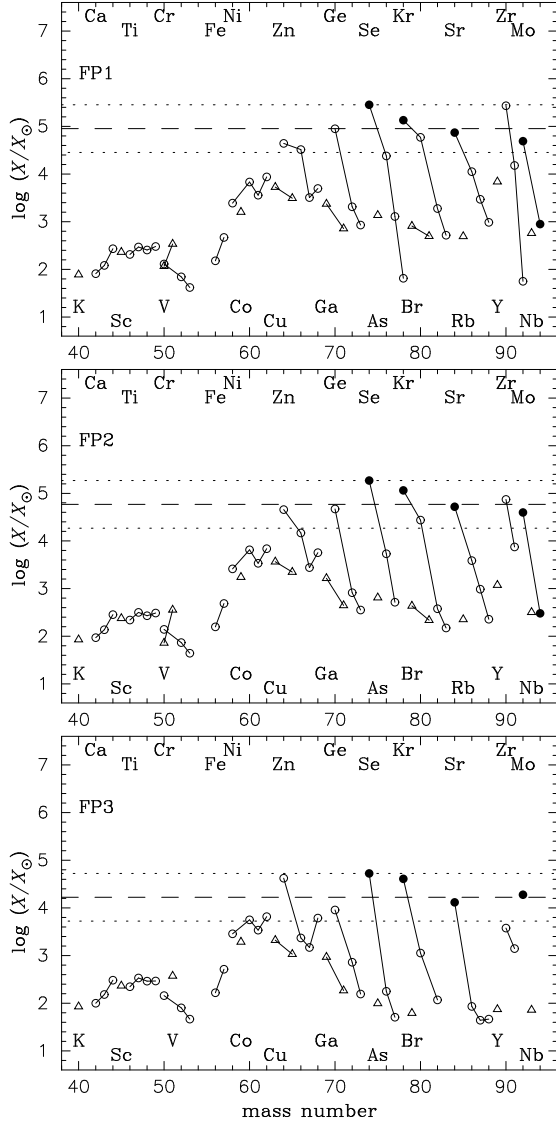


FIG. 11.— Same as Figure 4, but for models FP1 (*top*), FP2 (*middle*), and FP3 (*bottom*).

The νp -process (or neutrino-induced rp -process) is now believed to be a promising nuclear process that synthesizes light p -nuclei up to $A \sim 110$ (Fröhlich et al. 2006; Pruet et al. 2006; Wanajo 2006). In this process, a fraction of free protons are converted to neutrons by neutrino capture in the early proton-rich supernova ejecta. The β -waiting points on the classical rp -process path (e.g., ^{64}Ge with the half-life of 1.06 minutes) are then bypassed via much faster neutron capture. The current models contain proton-rich ejecta (up to 0.53, Figs. 1 and 3), where one may expect the occurrence of the νp -process.

The νp -process plays, however, no role in producing the p -nuclei, although all the examined models in this study include neutrino-induced reactions on free nucleons and α particles. In order to test the effect of neutrinos, the result without neutrino-induced reactions (labelled *no ν* , otherwise using the same input as in model ST) is compared with that of model ST (Fig. 7c). We find that neutron capture, which is absent without neutrino-induced reactions, diminishes the nuclei with $A \leq 20$. The mass fractions of these isotopes are, however, very

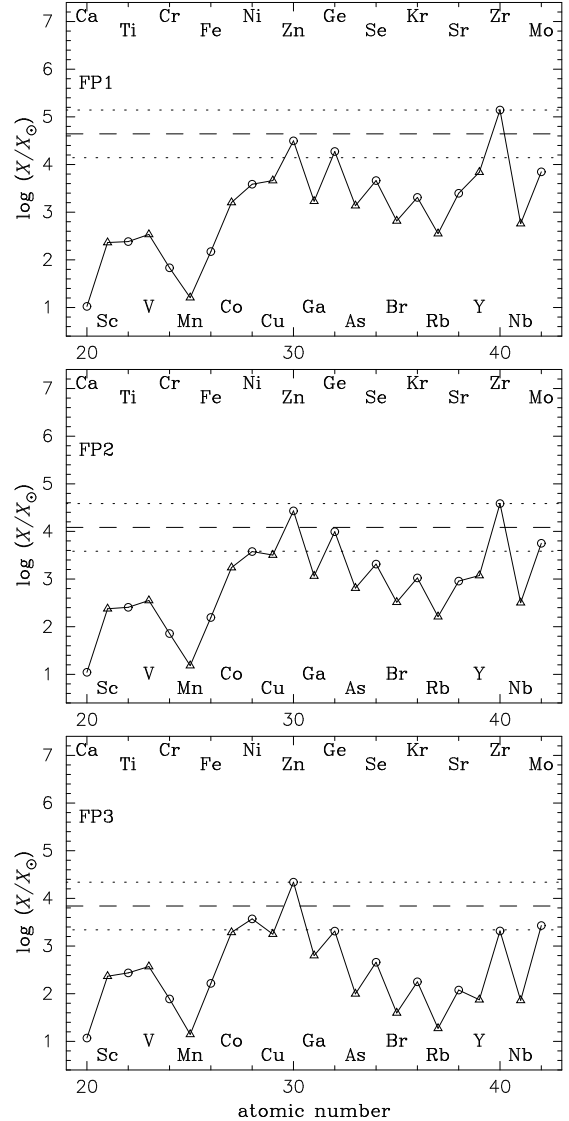


FIG. 12.— Same as Figure 5, but for models FP1 (*top*), FP2 (*middle*), and FP3 (*bottom*).

small compared to the dominant species at $A \approx 4, 60$, and 90. No substantial differences can be seen for the nuclei with $A > 50$ because of the moderate proton-richness (up to $Y_{e,i} = 0.53$), moderate entropy (up to $30 k_B$ per nucleon, where k_B is the Boltzmann constant), and the fast expansion of the ejecta. The proton-rich ejecta quickly cool down below $T_9 \approx 2 - 3$, which is the relevant temperature range for the νp -process to take place (i.e., the proton captures are fast and their inverse reactions slow). The νp -process might be efficient only in core-collapse supernovae from more massive progenitors (e.g., $\gtrsim 15 M_\odot$), which have a shallower density gradient at the core edge and a denser envelope and thus their explosions develop in a different way with different conditions for nucleosynthesis.

4. CONTRIBUTION TO GALACTIC CHEMICAL EVOLUTION

We now discuss a possible contribution of electron capture supernovae to Galactic chemical evolution. First, we suppose that model ST, which has the largest over-

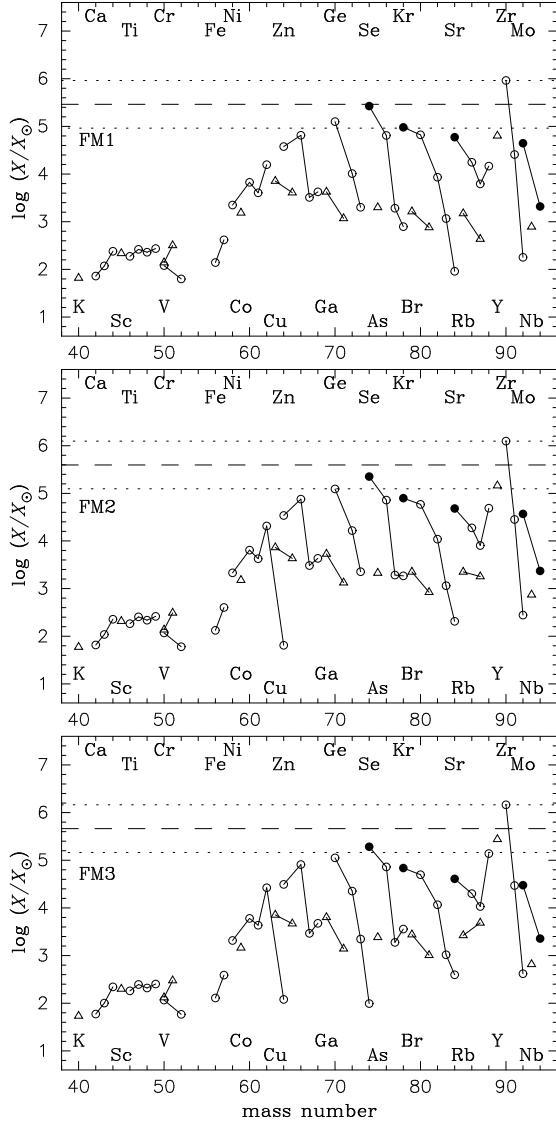


FIG. 13.— Same as Figure 4, but for models FM1 (*top*), FM2 (*middle*), and FM3 (*bottom*).

production factor for ^{90}Zr (Fig. 4), is representative of this type of supernovae. Let us assume that electron capture supernovae produce all ^{90}Zr in nature, and the other supernovae from the progenitors more massive than $10 M_{\odot}$ produce ^{16}O with a typical amount of $M_{\text{other}}(^{16}\text{O}) = 1.5 M_{\odot}$ per event. Here, $M_{\text{other}}(^{16}\text{O})$ is taken to be the initial-mass-function averaged yield of Nomoto et al. (2006) between 13 and $40 M_{\odot}$ (solar metallicity models). The contribution of electron capture supernovae to the Galactic ^{16}O is negligible (Table 2). If we assume the number fraction of electron capture supernovae relative to all core-collapse supernovae to be f_* , we have the relation

$$\frac{f_*}{1 - f_*} = \frac{X(^{90}\text{Zr})_{\odot}/X(^{16}\text{O})_{\odot}}{M(^{90}\text{Zr})/M_{\text{other}}(^{16}\text{O})} = 0.029, \quad (1)$$

where $X(^{16}\text{O})_{\odot} = 6.6 \times 10^{-3}$, $X(^{90}\text{Zr})_{\odot} = 1.5 \times 10^{-8}$ (Lodders 2003), and $M(^{90}\text{Zr}) = 1.2 \times 10^{-4} M_{\odot}$ (Table 1). Therefore we expect the frequency of electron capture supernovae to be no more than 1% of all core-collapse

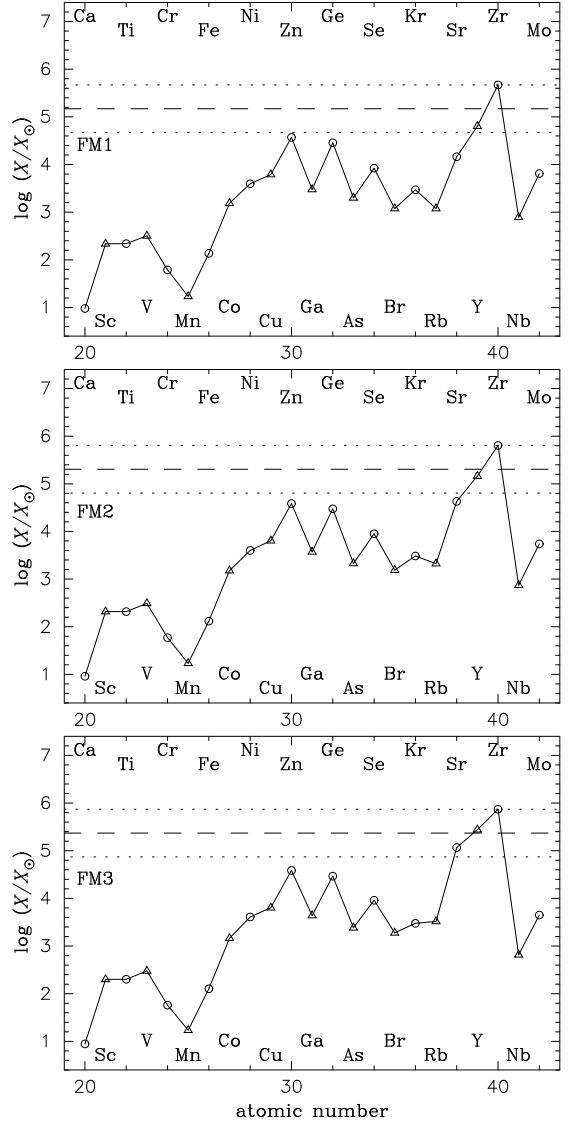


FIG. 14.— Same as Figure 5, but for models FM1 (*top*), FM2 (*middle*), and FM3 (*bottom*).

events, when taking into account that there are also other sources of ^{90}Zr (81% is from the *s*-process, Burris et al. 2000). As discussed in § 3.5, however, the production of ^{90}Zr is extremely sensitive to $Y_{e,i}$, changing more than 2 orders of magnitude with only 2% variation of $Y_{e,i}$ (Table 1). Thus, we do not consider the overproduction of ^{90}Zr to give a tight constraint on the occurrence of electron capture supernovae.

Instead, we propose the abundance of ^{64}Zn , whose production is insensitive to small variations of $Y_{e,i}$ (Table 1), to serve as a strong constraint on the occurrence of this type of supernovae. As an example, we consider model FP3 (Fig. 11; *bottom*) as representative of electron capture supernovae, in which the largest overproduction is shared by ^{64}Zn , ^{74}Se , and ^{78}Kr . The origins of these isotopes have not been well identified, although the latter two *p*-isotopes might be produced to some extent by the γ -process (Rayet et al. 1995) or νp -process (Fröhlich et al. 2006; Pruet et al. 2006; Wanajo 2006) in core-collapse supernovae. We therefore can as-

sume that all ^{64}Zn (and ^{74}Se , ^{78}Kr) in nature is produced by electron capture supernovae. In this case, equation (1) with ^{90}Zr replaced by ^{64}Zn gives $f_* = 0.28$, where $X(^{64}\text{Zn})_{\odot} = 1.1 \times 10^{-6}$ (Lodders 2003) and $M(^{64}\text{Zn}) = 6.5 \times 10^{-4} M_{\odot}$ (Table 1). We thus conclude that the upper limit of the frequency of electron capture supernovae is around 30% of all the core-collapse events. This is in good agreement with the upper limit estimated from a recent study of stellar evolution ($\sim 20\%$, Poelarends et al. 2008) as well as the estimate for the rate of SN 2008S-like transients ($\sim 20 - 30\%$, Thompson et al. 2008). Our result implies that a significant fraction of $8 - 10 M_{\odot}$ is allowed to enter into the supernova channel from the nucleosynthetic point of view.

For a practical use, the yields of all stable (Table 2) and some unstable (Table 3) isotopes for models ST and FP3 are presented. For the study of Galactic chemical evolution, one can use those of model FP3 as representative of electron capture supernovae, keeping in mind that the $Y_{e,i}$ profile (i.e., the initial composition) of this model was slightly modified. Nevertheless, it would be interesting to see if this type of supernovae was the dominant source of Zn and of the most mysterious p -nucleus ^{92}Mo . In fact, all the previous models of supernova nucleosynthesis (with typical explosion energy), except for *hypernovae* (Umeda & Nomoto 2002), have failed to explain the solar inventory of ^{64}Zn (which is the most abundant isotope of this element). We do not expect a substantial contribution to the abundance of ^{64}Zn from the later ($t_{\text{pb}} > 1$ s) neutrino-driven wind (Hoffman et al. 1996; Wanajo 2006), whose total mass is no more than $0.001 M_{\odot}$ with ^4He being the dominant species (e.g., Wanajo 2007). The p -isotope ^{92}Mo can be synthesized by the νp -process to some extent, but still falls a few times short of what is expected from the neighboring p -nuclei (^{84}Sr , ^{94}Mo , and $^{96,98}\text{Ru}$, Pruet et al. 2006; Wanajo 2006).

5. ORIGIN OF FAINT SUPERNOVAE?

Our result confirms that electron capture supernovae produce very little ^{56}Ni ($\approx 0.002 - 0.004 M_{\odot}$, Table 1) compared to $\sim 0.1 M_{\odot}$ in the case of more massive progenitors (e.g., Nomoto et al. 2006). This is a consequence of the small ejecta mass ($= 0.0139 M_{\odot}$ without the H-rich envelope) and also of the neutron-richness of the bulk of the ejecta ($Y_{e,i} < 0.49$ for mass shells in the range of $1.367 - 1.373 M_{\odot}$, Fig. 6), because of which ^{56}Ni is not a dominant species to be produced. The yield of ^{56}Ni , which is mainly created in matter with $Y_{e,i} \sim 0.5$, is insensitive to a small variation of Y_e (Table 1). We also do not expect a significant contribution from the later ($t_{\text{pb}} > 1$ s) neutrino wind. The uncertainty arising from the nuclear EoS seems larger than that from Y_e , being about a factor of 2 (Table 1) for the currently available versions of EoSs. The uncertainty might become larger if a variety of EoSs are available in the future. The convective motion near the mass cut may also affect the ^{56}Ni mass (§ 3.4), which needs multi-dimensional simulations.

The expected small amount of ^{56}Ni as well as the low explosion energy of electron capture supernovae have been proposed as an explanation of the observed properties of faint SNe II-P (e.g., SN 1997D, Chugai & Utrobin 2000; Kitaura et al. 2006) and of the low luminos-

ity of SN 2008S-like transients (possibly a new subclass of SNe II_n, Prieto et al. 2008; Thompson et al. 2008). The former ones, namely SNe 1994N, 1997D, 1999br, 1999eu, 2001dc, and 2005cs, have been observationally defined as the class of low-luminosity Ni-poor SNe II-P (Pastorello et al. 2004, 2006), whose incidence is estimated to be as high as 4 – 5% of all SNe II. The estimated ^{56}Ni masses of $\sim 0.002 - 0.008 M_{\odot}$ for these low-luminosity SNe II-P (Zampieri et al. 2003; Pastorello et al. 2004, 2006; Hendry et al. 2005) are in reasonable agreement with the present result from electron capture supernovae. An alternative possibility is the origin of such supernovae from much more massive stars ($\gtrsim 20 M_{\odot}$) with low explosion energies, which suffer from fallback of freshly synthesized ^{56}Ni (e.g., Turatto et al. 1998; Benetti et al. 2001; Nomoto et al. 2003; Zampieri et al. 2003). This is due to the inferred large envelope masses for the low-luminosity SNe II-P ($\sim 14 - 40 M_{\odot}$, Hendry et al. 2005) that favor massive progenitors. A recent analysis of the progenitors of SNe II-P by Smartt et al. (2008) indicates, however, that low-luminosity supernovae with low ^{56}Ni production are likely to arise from low mass progenitors near the minimum mass limit for core-collapse supernovae. A lack of α -elements such as O and Mg in the case of electron capture supernovae will be a key to spectroscopically distinguish between these two scenarios (Kitaura et al. 2006).

The Crab nebula (the relic of SN 1054) is known to have a low kinetic energy ($\sim 4 \times 10^{49}$ erg, Chevalier 1985) and a small amount of α -elements (Davidson et al. 1982). An electron capture supernova has been suggested to be the origin of the Crab nebula (Nomoto et al. 1982; Nomoto 1985; Kitaura et al. 2006). Our result with the little production of α -elements and iron supports this idea. The Ni/Fe ratios ($\approx 1 - 2$, except for the extreme model MX, Table 1), which are at least 20 times larger than the solar value ($= 0.058$) can be considered as an additional support, because they are in reasonable agreement with the reported high Ni/Fe ratio of the Crab nebula (~ 10 times solar; Henry 1984; Hudgins et al. 1990).

Recently, MacAlpine & Satterfield (2008) investigated gaseous regions of the Crab nebula and inferred from their photoionization calculations that the abundance of a large component of the nebula appears to be He-rich and $\text{C/O} > 1$. According to the $8 - 10 M_{\odot}$ star models (Nomoto et al. 1982; Nomoto 1984), the He-rich envelope for $M \lesssim 9.5 M_{\odot}$ has $\text{C/O} < 1$ because of the preceding CNO-cycle, while that for $M \gtrsim 9.5 M_{\odot}$ has $\text{C/O} > 1$ owing to the 3α -reactions. The $9.6 M_{\odot}$ star in Nomoto (1984, case 2.4), for example, has carbon and oxygen mass fractions of 0.022 and 0.0033 in the He-burning convective layer (corresponding solar values are 0.0025 and 0.0066, respectively; Lodders 2003). This enhanced carbon abundance (ten times that of the solar value) is consistent with that reported by MacAlpine & Satterfield (2008). It should be noted that stars with initial masses of $\sim 9.5 - 10 M_{\odot}$ have almost identical core structures to our considered star of $8.8 M_{\odot}$, except for the outermost oxygen mass fraction (Nomoto 1984, 1987). Therefore, the explosion of a star with an initial mass of $\sim 9.5 - 10 M_{\odot}$ and with an O-Ne-Mg core can be the origin of the Crab remnant.

We also note that the dredge-up of the material from

the He-layer into the H-layer enhances carbon in the envelope of the AGB star (Nomoto 1987). This would be more efficient in enhancing carbon than He-thermal pulses, and dust could be easily formed to induce mass loss. This may result in a deeply dust-enshrouded object such as the progenitor of SN 2008S (Prieto et al. 2008; Thompson et al. 2008). For the $9.6 M_{\odot}$ star in Nomoto (1984, case 2.4), the duration of the AGB phase is estimated to be 4×10^4 yr (that becomes shorter for a more massive case), which is in reasonable agreement with the inferred dust-enshrouded phase for SN 2008S-like transients ($\lesssim 10^4$ yr, Thompson et al. 2008). This might also imply the mass range of the stars that end their lives as electron capture supernovae to be $\sim 9.5 - 10 M_{\odot}$, whose frequency, $\sim 7 - 8\%$ of all the core-collapse events, satisfies the constraint from our nucleosynthesis results ($< 30\%$; § 4).

6. CONCLUSIONS

We have investigated the nucleosynthesis during the first 810 ms after core bounce in an explosion from a collapsing star with O-Ne-Mg core (electron capture supernova) and an initial mass of $8.8 M_{\odot}$. The thermodynamic trajectories are taken from the self-consistent explosion models of Kitaura et al. (2006), which were computed with the initial stellar model of Nomoto (1984, 1987). Our main conclusions can be summarized as follows.

1. Our unmodified model (ST) results in (i) little production of α -elements and iron, (ii) large production of ^{64}Zn , ^{70}Ge , and in particular, ^{90}Zr , and (iii) production of some light p -nuclei (^{74}Se , ^{78}Kr , ^{84}Sr , and ^{92}Mo). This is a consequence of the ejection of a sizable amount of neutron-rich matter ($6 \times 10^{-3} M_{\odot}$ with $Y_e = 0.46 - 0.49$). If we assume this model to be representative of electron capture supernovae, the occurrence of this type of supernovae is limited to be no more than 1% of all core-collapse events. We do not think, however, that the production of ^{90}Zr serves as a strong constraint, because it is easily affected by a small variation of Y_e . The νp -process does not play any role for the production of p -nuclei in the present supernova model.

2. The uncertainties in the nuclear EoS and the nuclear reaction rates do not substantially affect the nucleosynthesis results. In contrast, the effects of convection, which are not included in the one-dimensional simulations of Kitaura et al. (2006), are expected to be large and may change the initial Y_e distribution to some extent. The overproduction of ^{90}Zr is moderated if the minimum Y_e is only 1–2% larger than that in the unmodified model ST. In this case (our model FP3) the largest overproduction, which is observed for ^{64}Zn , ^{74}Se , and ^{78}Kr , is reduced to one tenth of that of the unmodified model. The robustness of the ^{64}Zn production against small variations of Y_e provides an upper limit to the occurrence of electron capture supernovae to be about 30% of all stellar core-collapse events. Electron capture supernovae can be significant contributors to the Galactic inventories of ^{64}Zn (the most abundant isotope of Zn) and some light

p -nuclei (e.g., ^{92}Mo), if the assumed slightly larger values of Y_e were correct.

3. The high Ni/Fe ratio ($= 1 - 2$) and the small production of α -elements, as well as the low explosion energy ($1 - 2 \times 10^{50}$ erg, Kitaura et al. 2006; Janka et al.

TABLE 1
YIELDS IN UNITS OF SOLAR MASSES

Model	$Y_{e,\text{min}}$	^{56}Ni	^{64}Zn	^{90}Zr	Ni/Fe
ST	0.464	2.50E-03	6.38E-04	1.21E-04	1.65
WH	0.462	4.06E-03	7.31E-04	1.39E-04	1.27
RT	0.464	2.52E-03	6.94E-04	7.83E-05	1.58
MX	0.480	1.67E-03	1.07E-03	3.32E-08	3.01
FP1	0.468	2.62E-03	6.83E-04	5.75E-05	1.55
FP2	0.471	2.76E-03	7.08E-04	1.59E-05	1.46
FP3	0.475	2.91E-03	6.51E-04	8.04E-07	1.36
FM1	0.460	2.41E-03	5.83E-04	1.96E-04	1.73
FM2	0.457	2.32E-03	5.31E-04	2.66E-04	1.82
FM3	0.453	2.24E-03	4.83E-04	3.11E-04	1.92

2008a,b), support the hypothesis that the Crab nebula is the remnant of an electron capture supernova (Nomoto et al. 1982; Davidson et al. 1982).

4. SN 2008S-like transients, whose progenitors are deeply dust-enshrouded massive stars, are likely to be electron capture supernovae of AGB stars. This implies that electron capture supernovae constitute a newly identified sub-class of SNe IIn (Prieto et al. 2008; Thompson et al. 2008).

5. The ejecta mass of ^{56}Ni is $0.002 - 0.004 M_{\odot}$, which is in reasonable agreement with estimates for observed low-luminosity supernovae. The amount might be, however, affected by the convective motion near the mass cut. Multi-dimensional studies will clarify the effect of convection on the production of ^{56}Ni as well as ^{90}Zr .

We are grateful to an anonymous referee for important comments. This research has been supported in part by World Premier International Research Center Initiative (WPI Initiative), MEXT, Japan, and by the Grant-in-Aid for Scientific Research of the JSPS (17740108, 18104003, 18540231, 20540226) and MEXT (19047004, 20040004). In Garching, the project was supported by the Deutsche Forschungsgemeinschaft through the Transregional Collaborative Research Centers SFB/TR 27 “Neutrinos and Beyond” and SFB/TR 7 “Gravitational Wave Astronomy”, and the Cluster of Excellence EXC 153 “Origin and Structure of the Universe” (<http://www.universe-cluster.de>). The computations were done at the Rechenzentrum Garching and at the High Performance Computing Center Stuttgart (HLRS) under grant number SuperN/12758.

REFERENCES

- Aikawa, M., Arnould, M., Goriely, S., Jorissen, A., & Takahashi, K. 2005, *A&A*, 441, 1195
- Audi, G., Wapstra, A. H., & Thibault, C. 2003, *Nucl. Phys. A*, 729, 337
- Baron, E., Cooperstein, J., & Kahana, S. 1987, *ApJ*, 320, 300

TABLE 2
YIELDS OF STABLE ISOTOPES (IN UNITS OF M_{\odot})

Species	ST	FP3	Species	ST	FP3
¹ H ...	5.55E-05	3.84E-05	⁵⁸ Ni ..	1.79E-03	2.21E-03
² H ...	1.98E-13	1.35E-13	⁶⁰ Ni ..	2.09E-03	1.72E-03
³ He ...	6.52E-10	6.49E-10	⁶¹ Ni ..	5.04E-05	4.62E-05
⁴ He ...	5.12E-03	5.55E-03	⁶² Ni ..	5.11E-04	2.88E-04
⁶ Li ...	6.70E-15	6.57E-15	⁶⁴ Ni ..	2.55E-07	5.38E-09
⁷ Li ...	4.52E-09	5.31E-09	⁶³ Cu ..	5.96E-05	1.97E-05
⁹ Be ...	2.05E-14	1.99E-14	⁶⁵ Cu ..	1.56E-05	4.59E-06
¹⁰ B ..	2.72E-14	2.45E-14	⁶⁴ Zn ..	6.38E-04	6.51E-04
¹¹ B ..	3.02E-09	3.34E-09	⁶⁶ Zn ..	4.54E-04	2.16E-05
¹² C ...	1.18E-06	1.48E-06	⁶⁷ Zn ..	4.44E-06	2.03E-06
¹³ C ..	6.82E-09	7.09E-09	⁶⁸ Zn ..	2.89E-05	3.90E-05
¹⁴ N ..	5.54E-08	4.08E-08	⁷⁰ Zn ..	9.72E-12	2.14E-14
¹⁵ N ..	1.02E-07	8.25E-08	⁶⁹ Ga ..	1.93E-06	5.68E-07
¹⁶ O ...	1.03E-07	1.13E-07	⁷¹ Ga ..	3.96E-07	7.64E-08
¹⁷ O ...	5.17E-11	5.33E-11	⁷⁰ Ge ..	8.29E-05	6.61E-06
¹⁸ O ...	7.16E-09	5.41E-09	⁷² Ge ..	5.05E-06	7.10E-07
¹⁹ F ..	1.02E-08	8.95E-09	⁷³ Ge ..	4.11E-07	4.32E-08
²⁰ Ne..	3.12E-08	4.08E-08	⁷⁴ Ge ..	5.16E-09	6.86E-12
²¹ Ne..	1.63E-10	2.00E-10	⁷⁶ Ge ..	2.91E-14	4.90E-20
²² Ne..	5.37E-09	5.82E-09	⁷⁵ As ..	3.35E-07	1.84E-08
²³ Na..	3.33E-10	4.46E-10	⁷⁴ Se ..	5.13E-06	9.28E-07
²⁴ Mg .	1.80E-08	2.53E-08	⁷⁶ Se ..	9.05E-06	3.39E-08
²⁵ Mg .	5.30E-09	1.05E-08	⁷⁷ Se ..	2.77E-07	7.99E-09
²⁶ Mg .	4.40E-08	4.30E-08	⁷⁸ Se ..	1.32E-07	5.41E-11
²⁷ Al ..	3.03E-09	3.32E-09	⁸⁰ Se ..	1.49E-10	2.87E-14
²⁸ Si ...	5.44E-08	8.45E-08	⁸² Se ..	8.40E-16	0.00E+00
²⁹ Si ...	1.11E-08	1.66E-08	⁷⁹ Br ..	2.08E-07	1.15E-08
³⁰ Si ...	6.82E-08	6.13E-08	⁸¹ Br ..	1.23E-07	3.09E-09
³¹ P ...	2.10E-08	2.82E-08	⁷⁸ Kr ..	7.06E-07	2.58E-07
³² S ...	1.98E-07	2.76E-07	⁸⁰ Kr ..	2.88E-06	4.71E-08
³³ S ...	3.37E-08	3.89E-08	⁸² Kr ..	1.08E-06	2.53E-08
³⁴ S ...	2.27E-07	2.20E-07	⁸³ Kr ..	2.03E-07	5.58E-09
³⁶ S ...	4.09E-12	5.03E-12	⁸⁴ Kr ..	3.57E-08	6.87E-12
³⁵ Cl ..	1.78E-07	2.03E-07	⁸⁶ Kr ..	1.24E-11	3.48E-18
³⁷ Cl ..	1.05E-07	1.14E-07	⁸⁵ Rb ..	1.40E-07	4.29E-09
³⁶ Ar ..	1.11E-06	1.41E-06	⁸⁷ Rb ..	4.21E-09	1.39E-15
³⁸ Ar ..	2.62E-07	3.01E-07	⁸⁴ Sr ..	3.10E-07	5.87E-08
⁴⁰ Ar ..	9.90E-11	1.24E-10	⁸⁶ Sr ..	1.29E-06	6.94E-09
³⁹ K ..	4.07E-07	4.83E-07	⁸⁷ Sr ..	2.92E-07	2.72E-09
⁴⁰ K ..	4.98E-10	5.98E-10	⁸⁸ Sr ..	2.74E-06	3.24E-08
⁴¹ K ..	8.14E-08	8.53E-08	⁸⁹ Y ..	3.92E-06	1.25E-08
⁴⁰ Ca..	3.55E-06	3.93E-06	⁹⁰ Zr ..	1.21E-04	8.04E-07
⁴² Ca..	5.23E-07	6.98E-07	⁹¹ Zr ..	9.96E-07	6.61E-08
⁴³ Ca..	1.77E-07	2.27E-07	⁹² Zr ..	7.81E-09	1.35E-10
⁴⁴ Ca..	5.96E-06	7.17E-06	⁹⁴ Zr ..	3.89E-16	1.97E-20
⁴⁶ Ca..	2.44E-15	1.25E-15	⁹⁶ Zr ..	0.00E+00	0.00E+00
⁴⁸ Ca..	0.00E+00	0.00E+00	⁹³ Nb ..	2.05E-08	2.07E-09
⁴⁵ Sc..	1.41E-07	1.46E-07	⁹² Mo .	7.02E-07	2.73E-07
⁴⁶ Ti ..	7.18E-07	8.29E-07	⁹⁴ Mo .	1.42E-08	2.32E-10
⁴⁷ Ti ..	9.24E-07	1.17E-06	⁹⁵ Mo .	7.96E-11	1.16E-11
⁴⁸ Ti ..	8.36E-06	1.01E-05	⁹⁶ Mo .	3.94E-12	6.44E-14
⁴⁹ Ti ..	7.47E-07	7.64E-07	⁹⁷ Mo .	1.46E-12	2.09E-13
⁵⁰ Ti ..	3.35E-12	7.44E-14	⁹⁸ Mo .	6.96E-18	0.00E+00
⁵⁰ V ..	1.94E-09	2.97E-10	¹⁰⁰ Mo	0.00E+00	0.00E+00
⁵¹ V ..	1.95E-06	2.23E-06	⁹⁶ Ru ..	2.59E-11	1.58E-11
⁵⁰ Cr ..	1.41E-06	1.64E-06	⁹⁸ Ru ..	2.86E-12	6.57E-14
⁵² Cr ..	1.50E-05	1.82E-05	⁹⁹ Ru ..	1.70E-14	8.73E-16
⁵³ Cr ..	1.04E-06	1.22E-06	¹⁰⁰ Ru .	7.23E-15	4.99E-16
⁵⁴ Cr ..	1.26E-08	1.86E-09	¹⁰¹ Ru .	2.58E-16	2.17E-17
⁵⁵ Mn .	3.41E-06	2.88E-06	¹⁰² Ru .	9.02E-19	0.00E+00
⁵⁴ Fe .	3.22E-06	3.64E-06	¹⁰⁴ Ru .	0.00E+00	0.00E+00
⁵⁶ Fe ..	2.52E-03	2.92E-03	¹⁰³ Rh .	4.39E-18	1.01E-19
⁵⁷ Fe ..	1.80E-04	2.13E-04	¹⁰² Pd .	3.81E-16	1.65E-17
⁵⁸ Fe ..	7.25E-08	2.18E-08	¹⁰⁴ Pd .	3.19E-18	4.54E-21
⁵⁹ Co ..	8.61E-05	1.08E-04	¹⁰⁵ Pd .	1.52E-20	0.00E+00

TABLE 3
YIELDS OF UNSTABLE ISOTOPES (IN UNITS OF M_{\odot})

Species	ST	FP3	Species	ST	FP3
²² Na..	5.37E-09	5.81E-09	⁶⁰ Fe ..	1.40E-14	4.79E-16
²⁶ Al ..	3.27E-08	2.97E-08	⁵⁶ Ni ..	2.50E-03	2.91E-03
⁴¹ Ca..	8.05E-08	8.43E-08	⁵⁷ Ni ..	1.77E-04	2.11E-04
⁴⁴ Ti ..	5.96E-06	7.17E-06	⁹² Nb..	6.35E-09	1.34E-10

- Benetti, S., et al. 2001, MNRAS, 322, 361
- Burris, D. L., Pilachowski, C. A., Armandroff, T. E., Sneden, C., Cowan, J. J., & Roe, H. 2000, ApJ, 544, 302
- Burrows, A. & Lattimer, J. M. 1985, ApJ, 299, L19
- Burrows, A., Dessart, L., & Livne, E. 2007, in AIP Conf. Ser. 937, Supernova 1987A: 20 Years After, ed. S. Immler & R. McCray (New York: AIP), 370
- Buras, R., Rampp, M., Janka, H. -Th, & Kifonidis, K. 2006, A&A, 447, 1049
- Chevalier, R. A. 1985, in The Crab Nebula and Related Supernova Remnants, ed. M. C. Kafatos & R. B. C. Henry (Cambridge: Cambridge Univ. Press), 63
- Chugai, N. N., & Utrobin, V. P. 2000, A&A, 354, 557
- Davidson, K., et al. 1982, ApJ, 253, 696
- Fröhlich, C., et al. 2006, ApJ, 637, 415
- Fuller, G. M., Fowler, W. A., & Newman, M. J. 1982, ApJS, 48, 279
- Graboske, H. C., Dewitt, H. E., Grossman, A. S., Cooper, M. S. 1973, ApJ, 181, 457
- Goriely, S., Samyn, M., Pearson, J. M., & Onsi, M. 2005, Nucl. Phys. A, 750, 425
- Heger, A. & Woosley, S. E. 2008, ApJ, submitted (arXiv:0803.3161)
- Hendry, M. A., et al. 2005, MNRAS, 359, 906
- Henry, R. B. C. 1984, ApJ, 281, 644
- Hillebrandt, W. 1982, A&A, 110, L3
- Hillebrandt, W., Nomoto, K., & Wolff, G. 1984, A&A, 133, 175
- Hoffman, R. D., Woosley, S. E., Fuller, G. M., & Meyer, B. S. 1996, ApJ, 460, 478
- Hoffman, R. D., Müller, B., & Janka, H. -T. 2008, ApJ, 676, L127
- Hudgins, S., Herter, T., & Joyce, R. J. 1990, ApJ, 354, L57
- Janka, H. -Th., Müller, B., Kitaura, F. -S., & Buras, R. 2008a, A&A, 485, 199
- Janka, H. -Th., Marek, A., Müller, B., & Scheck, L. 2008b, in *40 Years of Pulsars: Millisecond Pulsars, Magnetars, and More*, Proc. Int. Conf., McGill Univ., Montreal, Canada, August 12-17, 2007, Eds. C.G. Bassa, Z. Wang, A. Cumming, and V. Kaspi, AIP Conference Proceedings, Vol. 983, American Institute of Physics, New York, p. 369; arXiv:0712.3070
- Kitaura, F. S., Janka, H. -Th., & Hillebrandt, W. 2006, A&A, 450, 345
- Langanke, K. & Martinez-Pinedo, G. 2001, At. Data Nucl. Data Tables, 79, 1
- Lattimer, J., & Swesty, F. 1991, Nucl. Phys. A, 535, 331
- Liebrandt, M., Mezzacappa, A., Thielemann, F. -K., Messer, O. E. Hix, W. R., & Bruenn, S. W. 2001, Phys. Rev. D, 63, 103004
- Lodders, K. 2003, ApJ, 591, 1220
- MacAlpine, G. M. & Satterfield, T. J. 2008, AJ, submitted; arXiv:0806.1342
- Mayle, R. & Wilson, J. R. 1988, ApJ, 334, 909
- McLaughlin, G. C., Fuller, G. M., & Wilson, J. R. 1996, ApJ, 472, 440
- Meyer, B. S., Krishnan, T. D., & Clayton, D. D. 1998, ApJ, 498, 808
- Meyer, B. S., McLaughlin, G. C., & Fuller G. M. 1998, Phys. Rev. C, 58, 3696
- Mezzacappa, A., Liebrandt, M., Messer, O. E., Hix, W. R., Thielemann, F. -K., & Bruenn, S. W. 2001, Phys. Rev. Lett., 86, 1935
- Miyaji, S., Nomoto, K., Yokoi, K., & Sugimoto, D. 1980, PASJ, 32, 303
- Nomoto, K., Sparks, W. M., Fesen, R. A., Gull, T. R., Miyaji, S., & Sugimoto, D. 1982, Nature, 299, 803
- Nomoto, K. 1984, ApJ, 277, 791

- Nomoto, K. 1985, in *The Crab Nebula and Related Supernova Remnants*, ed. M. C. Kafatos & R. B. C. Henry (Cambridge: Cambridge Univ. Press), 97
- Nomoto, K. 1987, *ApJ*, 322, 206
- Nomoto, K., Maeda, K., Umeda, H., Ohkubo, T., Deng, J., & Mazzali, P. 2003, in *IAU Symp. 212, A Massive Star Odyssey*, ed. V. D. Hucht, A. Herrero, & C. Esteban (San Francisco: ASP), 395
- Nomoto, K., Tominaga, N., Umeda, H., Kobayashi, C., & Maeda, K. 2006, *Nucl. Phys. A*, 777, 424
- Pastorello, A., et al. 2004, *MNRAS*, 347, 74
- Pastorello, A., et al. 2006, *MNRAS*, 370, 1752
- Pastorello, A., et al. 2007, *Nature*, 449, 1
- Poelarends, A. J. T., Herwig, F., Langer, N., & Heger, A. 2008, *ApJ*, 675, 614
- Prieto, J. L., et al. 2008, *ApJ*, 681, L9
- Pruet, J., Hoffman, R. D., Woosley, S. E., Janka, H. -Th., & Buras, R. 2006, *ApJ*, 644, 1028
- Rampp, M. & Janka, H. -T. 2000, *ApJ*, 539, L33
- Rayet, M., Arnould, M., Hashimoto, M., Prantzos, N., & Nomoto, K. 1995, *A&A*, 298, 517
- Rauscher, T. & Thielemann, F. -K. 2000, *At. Data Nucl. Data Tables*, 75, 1
- Shen, H., Toki, H., Oyamatsu, K., & Sumiyoshi, K. 1998, *Nucl. Phys. A*, 637, 435
- Siess, L. 2007, *A&A*, 476, 893
- Smartt, S. J., Eldridge, J. J., Crockett, R. M., & Maund, J. R. 2008, *MNRAS*, submitted; arXiv:0809.0403
- Sumiyoshi, K., Yamada, S., Suzuki, H., Shen, H., Chiba, S., & Toki, H. 2005, *ApJ*, 629, 922
- Tachibana, T., Yamada, M., & Yoshida, Y. 1990, *Progr. Theor. Phys.*, 84, 641
- Tominaga, N., Umeda, H., & Nomoto, K. 2007, *ApJ*, 660, 516
- Thompson, T. A., Burrows, A., & Pinto, P. A. 2003, *ApJ*, 592, 434
- Thompson, T. A., Prieto, J. L., Stanek, K. Z., Kistler, M. D., Beacom, J. F., & Kochanek, C. S. 2008, *ApJ*, submitted; arXiv:0809.0510
- Turatto, M., et al. 1998, *ApJ*, 498, L129
- Umeda, H. & Nomoto, K. 2002, *ApJ*, 565, 385
- Wanajo, S., Tamamura, M., Itoh, N., Nomoto, K., Ishimaru, Y., Beers, T. C., & Nozawa, S. 2003, *ApJ*, 593, 968
- Wanajo, S. 2006, *ApJ*, 647, 1323
- Wanajo, S. 2007, *ApJ*, 666, L77
- Woosley, S. E., Hartmann, D. H., Hoffman, R. D., & Haxton, W. C. 1990, *ApJ*, 356, 272
- Woosley, S. E., Wilson, J. R., Mathews, G. J., Hoffman, R. D., & Meyer, B. S. 1994, *ApJ*, 433, 229
- Zampieri, L., et al. 2003, *MNRAS*, 338, 711